A Validation Study on the Simultaneous Quantification of Multiple Wine Aroma Compounds with Static Headspace-Gas Chromatography-Ion Mobility Spectrometry (SHS-GC-IMS)

Wenyao Zhu[1,2], Frank Benkwitz[2], Paul A. Kilmartin[1]

[1] Wine Science Programme, The University of Auckland, Private Bag 92019, Auckland, 1142, New Zealand

[2] Kim Crawford Winery, Constellation Brands NZ, 237 Hammerichs Road, Blenheim, 7273, New Zealand

Abstract

A new quantitative method based on static headspace–gas chromatography–ion mobility spectrometry (SHS–GC–IMS) is proposed, which enables the simultaneous quantification of multiple aroma compounds in wine. The method was first evaluated for its stability and the necessity of using internal standards as a quality control measure. The two major hurdles in applying GC-IMS in quantification studies, namely, non-linearity and multiple ion species, were also investigated using the Boltzmann function and generalized additive model (GAM) as potential solutions. Metrics characterizing the model performance, including root mean squared error, bias, limit of detection, limit of quantification, repeatability, reproducibility, and recovery were investigated. Both non-linear fitting methods, Boltzmann function and GAM, were able to return desirable analytical outcomes with an acceptable range of error. A potential pitfall that would cause inaccurate quantification *i.e.*, competitive ionization, is also discussed. These findings provide an initial validation of a GC-IMS-based quantification method, as well as a starting point for further enhancing the analytical scope of GC-IMS.

Keywords

static headspace–gas chromatography–ion mobility spectrometry (SHS–GC–IMS), method development, method validation, quantitative analysis, Boltzmann function, generalized additive model (GAM), competitive ionization

1 Introduction

Being a separation technology that has only been commercialized in recent years, gas chromatography coupled with ion mobility spectrometry (GC-IMS) has rapidly gathered attention of researchers, especially from the field of food and beverage science.[1] Multiple studies have successfully applied GC-IMS for identifying food adulteration[2-4], optimizing food processing and storage conditions[5-7], assigning food origins[8-9], differentiating food quality gradings[10-11], and detecting food spoilage[12-13]. The majority of these findings have been summarized in a review article published in 2020.[14] GC-IMS is greatly appreciated for its ability to perform true orthogonal two-dimensional analyses, which considerably enhances the analytical capacity. This feature also enables non-targeted analyses that overcomes the need of prior peak identification and indifferently processes all peak information, which has been proven immensely helpful in establishing prediction models.[10-11]

Nevertheless, it remains that the major focus of research still centers around the qualitative and semi-quantitative use of the instrument, whereas quantitative studies using GC-IMS are still quite rare. Compared to gas chromatography-mass spectrometry (GC-MS), for which well-established protocols of quantitative method development are available, consensus is still to be reached even on some fundamental aspects in quantitative GC-IMS, such as the choice of curve-fitting functions[15-17], and the inclusion of internal standards during calibration[16-18]. A brief summary of recently published research articles describing the quantitative use of GC-IMS in various matrices is presented in **Table 1**. It is apparent that considerable discrepancies exist regarding GC-IMS-based quantification. Indeed, only recently has a publication regarding the practical considerations when dedicating GC-IMS for routine analyses became available[1], and protocols for GC-IMS method development are not well defined.

Furthermore, the quantification procedures of GC-IMS differ greatly to those of GC coupled to conventional detectors, such as the flame ionization detector (FID) and mass spectrometer (MS). This can be exemplified by the more confined linear dynamic ranges in GC-IMS outputs, which render the use of non-linear functions necessary over a wider concentration range. Such phenomena could be explained by the ionization source in IMS (radioactive atmospheric pressure chemical ionization, R-APCI), in addition to the formation of high-order oligomers and heterodimers with other compounds as the target compound concentration increases, thereby resulting in the plateauing of the current ion species.[1, 19] In addition, the instrumental response of the monomeric ion species does not conform to monotonic increase. Rather, it would begin to decrease as the compound concentration continues to increase and the dimer intensity becomes stronger, as illustrated in **Figure 1**. It hence presents an analytical hurdle in feasibly combining the information of multiple product ions pertaining to the same compound to approach more accurate quantification. Moreover, the non-linear nature of standard curves in GC-IMS further complicates the calculation of the figures of merit that are desired in method development, such as limit of detection (LOD) and limit of quantification (LOQ).

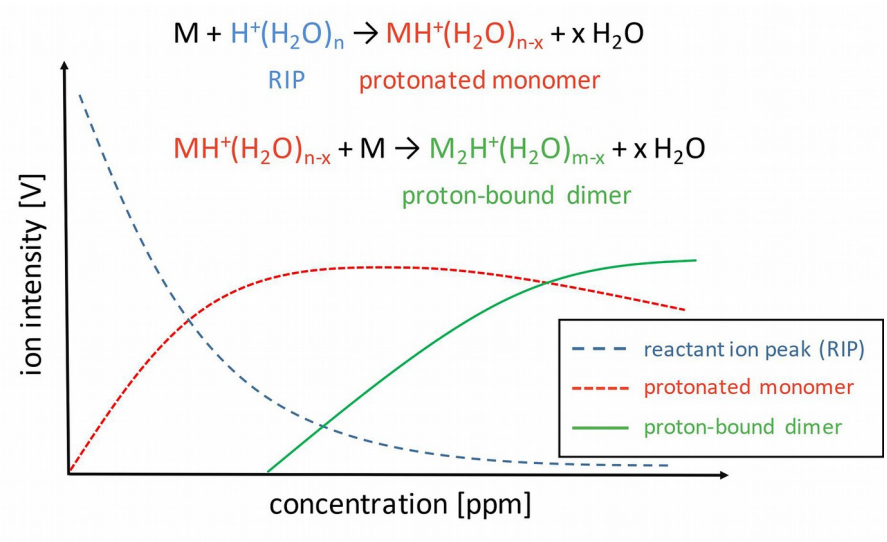

Figure 1. A schematic signal-concentration relationship curve of the monomer and dimer ions of a given compound in IMS detectors. Reprinted from *Chemometrics and Intelligent Laboratory Systems*, 205, Rebecca Brendel, Sebastian Schwolow, Sascha Rohn, Philipp Weller, Comparison of PLSR, MCR-ALS and Kernel-PLSR for the quantification of allergenic fragrance compounds in complex cosmetic products based on nonlinear 2D GC-IMS data, 104128, Copyright (2020), with permission from Elsevier.

To date, and to the best of our knowledge, no peer-reviewed article has been published in attempt to systematically discuss and provide a general solution to GC-IMS-based quantification methods. Therefore, the purpose of the current paper is to propose an initial approach to address the common hurdles during the development of quantitative methods using GC-IMS systems. Also, the possibility of utilizing multiple ion species (*e.g.*, monomer and dimer) will be discussed for further improving the method accuracy and sensitivity. As a preliminary trial, the method was used to establish calibration models for several volatile compounds commonly found in wine, as have been previously identified in our earlier study[11]. The analytical performance of this method was assessed using conventional ideas and some new tools that specifically tackle issues linked to GC-IMS.

Table 1. Summary of recent research publications on applying GC-IMS in quantitative analyses of volatile compounds.

Matrix of interest	Quantification method	Figures of merit (e.g., LOD, LOQ, recovery)	Number of quantified compounds	Use of internal standard	Ref.
yeast extract	relative semi-quantification adjusted against internal standard concentration	none reported	52	yes	20
white bread	dilution series of external standards without matrix and fitted to Boltzmann and linear functions	goodness-of-fit; linear range	44	not reported	16
heat- and acid-modified bovine dairy mix	dilution series of external standards in the original matrix and fitted to linear function	LOD; LOQ; recovery; precision	11	not reported	17
red wine (made from *Vitis amurensis*)	relative semi-quantification adjusted against internal standard concentration	none reported	46	yes	21

sunflower oil	dilution series of external standards in the original matrix data processed with spectrum unfolding coupled with multivariate regression methods: MCR-ALS and (*k*-) PLSR	standard error of prediction (SEP); relative percentage error of prediction (RE)	2	not reported	22
pathogenic fungi	dilution series of nebulized mix of external standards without matrix and fitted to linear function	LOD; LOQ; linear dynamic range; precision	14	not reported	23
olive oil	dilution series of the external standard (ethanol) in simulated matrix and fitted to linear and logarithmic functions	LOD; LOQ; precision	1	not reported	15
Natural and artificial fabrics	dilution series of external standards in simulated matrix and fitted to linear and polynomial functions	LOD; LOQ; goodness-of-fit; linear dynamic range	30		24
electronic cigarette liquid	dilution series of external standards in methanol/water matrix and fitted to linear and polynomial functions	LOD; LOQ; calibration range; goodness-of-fit	8	not reported	18

2 Materials and Methods

2.1 Chemicals, reference standards and wine samples

A total of 17 compounds were calibrated in the current study, including six acetate esters (methyl acetate, propyl acetate, isobutyl acetate, isoamyl acetate, amyl acetate, hexyl acetate), seven ethyl esters (ethyl propionate, ethyl butyrate, ethyl 2-methylbutyrate, ethyl isovalerate, ethyl hexanoate, ethyl octanoate, ethyl decanoate) and four higher alcohols (isobutanol, 1-butanol, isoamyl alcohol, 1-hexanol). Analytical standards (≥98% purity) of these compounds were procured from Sigma-Aldrich (Taufkirchen, BY, Germany) and were stored in a 5 °C cool room prior to use.

A model solution that mimics wine matrix was first prepared by dissolving 12% *v/v* ethanol in Type 1 water with pH adjusted to 3.2 by tartaric acid. The ethanol used was of HPLC grade purchased from Thermo Fisher Scientific (Auckland, New Zealand). This solution was later used to build the calibration models of the volatile compounds.

An internal standard (IS) working solution was prepared by diluting 3-octanol analytical standard in HPLC grade ethanol. For each sample analyzed using the SHS-GC-IMS instrument, an aliquot of 50 µL was spiked as a quality control. The IS working solution was prepared so that the absolute amount of 3-octanol in the spiked sample was 10–15 ppm.

For the precision trials, vintage 2018 commercial Sauvignon Blanc wine was used. For all other trials, vintage 2020 commercial Sauvignon Blanc wine was used. All wines used in the current study were produced in Marlborough, New Zealand, and had been stored in their original packaging and away from direct sunlight at room temperature before analysis.

2.2 Construction and validation of calibration models for volatile compounds

2.2.1 Preparation of calibration dilution series using analytical standards

In order to establish the calibration models for the aforementioned volatile compounds, stock solutions of each compound were first made by dissolving one drop (approximately 0.01 g) of the analytical standard into 5 mL ethanol. Serial dilutions were then made by dispensing the corresponding volumes of stock solution into the model solution to make up for the final analysis-ready volume of 5 mL. The IS working solution was spiked into each sample, followed by nitrogen purge of the headspace prior to instrument analyses. Each volatile was analyzed in their common ranges as typically found in white wines. Given the non-linear nature of the instrumental response, particular attention was paid to increase the number of calibration points, such that the curvature can be more accurately depicted. In the current study, at least eight calibration points (excluding zero points where only pure model solution was analyzed) were tested for each volatile compound.

2.2.2 Fitting of standard curves

Since SHS-GC-IMS features a small dynamic range, a non-linear standard curve is often necessary to depict the relationship between the compound concentration and the instrument response. According to the instrument manufacturer recommendations, the Boltzmann function is useful when considering the concentration-response relationship for the dimer ion of a compound. The Boltzmann function features the following generic form:

$$y = b + \frac{a - b}{1 + e^{\frac{\ln(x) - c}{d}}} \quad (1)$$

where *a*, *b*, *c*, *d* are constant coefficients, *y* = the signal intensity (volume-under-area-minimum, *a.u.*), *x* = analyte concentration (µg/L or mg/L). This function originated from the mathematical relationship of non-equilibrium thermodynamics and can also be used to depict ions travelling along an electric gradient.

Another method named the generalized additive model (GAM) was also used to simultaneously consider the signals of both monomer and dimer ions for predicting the compound concentration. GAM is a nonparametric method that directly reads the data without predefining a fixed mathematical expression for the concentration-response relationship. The main concept behind GAM can be expressed as:

$$g\left(E\left[y\middle|X\right]\right)=A_i\theta+f_1\left(x_1\right)+f_2\left(x_2\right)+f_3\left(x_3\right)+\ldots+f_i\left(x_i\right)+\epsilon \quad (2)$$

where $g\left(E\left[y\middle|X\right]\right)$ represents the expectation of the dependent variable *y* from a matrix of independent variables *X* as modelled by the link function (identity function in the case of regression); $A_i\theta$ is the parametric terms of the independent variable; $f_i\left(x_i\right)$ is the *i*-th term of the independent variable modelled using spline functions; ϵ is the intercept term. According to Hastie, Tibshirani and Friedman, a spline function is a piecewise polynomial function that is smooth in connecting knots between polynomial pieces.[25] Thus, this method utilizes a combination of basis spline functions to map the non-linear trend of calibration data points.

Alternatively, the investigated concentration range for some compounds still approximate a linear response range, in which case the linear fitting was also assessed for its characterization of the concentration-response relationship.

The goodness-of-fit of different fitting methods was evaluated using the root mean squared error (RMSE) and the systematic error (bias) as calculated using Equations 3 and 4.[22] Both metrics have the same unit as the concentration of the calibrated compound.

$$RMSE=\sqrt{\frac{\sum_{i=1}^{n}\left(c_i-c_i^{reg}\right)^2}{n}} \quad (3)$$

$$Systematic\,error=\frac{\sum_{i=1}^{n}\left(c_i^{reg}-c_i\right)}{n} \quad (4)$$

2.2.3 Limit of detection (LOD) and limit of quantification (LOQ)

Given the non-linear feature of the Boltzmann function, the conventional method of estimating the LOD and LOQ using the slope of the linear standard curve is not applicable. Hence, the current study adopted the methods described by Hayashi *et al.* and González *et al.* that enable the calculation of LOD and LOQ from non-linear calibration functions [26-27]. This method considers the relative standard deviation of the back-calculated analyte concentrations (denoted as ρ_x) and the first-order derivative of the original function (denoted as D). It is mandated that $\rho_x=\left|\sigma_y/x\cdot D\right|=30\,\%$ when LOD is reached and $\rho_x=20\,\%$ when LOQ is reached. σ_y is the standard error of instrument response estimates. y_i and y_i^{reg} represents the actual instrument response and the predicted instrument response, respectively. In the case of Boltzmann functions:

$$D\big|_{Boltzmann}=\frac{(b-a)\cdot e^{\frac{\ln(x)-c}{d}}}{d\cdot x\left(e^{\frac{\ln(x)-c}{d}}+1\right)^2} \tag{5}$$

$$\sigma_y\big|_{Boltzmann}=\sqrt{\frac{\sum_{i=1}^{n}\left(y_i-y_i^{reg}\right)^2}{n-4}} \tag{6}$$

Hence, the LOD and LOQ can be calculated as follows:

$$Let: P=\left[\frac{0.3(b-a)}{d\cdot\sigma_y}-2\right]\wedge Q=\left[\frac{0.2(b-a)}{d\cdot\sigma_y}-2\right] \tag{7}$$

$$LOD\big|_{Boltzmann}=e^c\cdot\left(\frac{P+\sqrt{P^2-4}}{2}\right)^d \tag{8}$$

$$LOQ\big|_{Boltzmann}=e^c\cdot\left(\frac{Q+\sqrt{Q^2-4}}{2}\right)^d \tag{9}$$

Since the method applies universally to both linear and non-linear standard curves, it was used to calculate the LOD and LOQ for all Boltzmann and linear fittings. In the case of linear standard curves with the generic form of $y=kx+m$, the LOD and LOQ calculations are as follows:

$$\sigma_y\big|_{linear}=\sqrt{\frac{\sum_{i=1}^{n}\left(y_i-y_i^{reg}\right)^2}{n-2}} \tag{10}$$

$$LOD\big|_{linear}=\frac{\sigma_y\big|_{linear}}{0.3k} \tag{11}$$

$$LOQ\big|_{linear}=\frac{\sigma_y\big|_{linear}}{0.2k} \tag{12}$$

Another method suggested by the International Union of Pure and Applied Chemistry (IUPAC) was also considered.[28-29] This method calculates the LOD and LOQ as follows:

$$LOD=\bar{y}+K_D\times\sigma \tag{13}$$

$$LOQ=\bar{y}+3\times K_D\times\sigma \tag{14}$$

$$K_D=t(\nu,\alpha)\times\sqrt{1+\frac{1}{n_B}} \tag{15}$$

In equations (13) to (15),n_B is the number of blank samples for a particular calibration and $t(\nu,\alpha)$ is the student-t distribution value of degrees of freedom (calculated as n_B-1,) and confidence interval of α (set as 0.05).[28] Since this method does not involve the inspection of the original mathematical equation, it thus provides an approach to calculate LOD and LOQ in GAM applications, although in the current study it was also tested on Boltzmann- and linear-based models.

2.2.4 Repeatability and reproducibility

The repeatability and reproducibility of the SHS-GC-IMS method in terms of retention and drift times has been previously reported in our previous study. Hence, in the current study special focus was placed on the repeatability and reproducibility of the quantification results, while employing the same data reported in the previous study.[11] A moderately aged (vintage 2018) Sauvignon Blanc wine was analyzed in quadruplicates per day for five days. The repeatability and reproducibility were calculated as intra- and inter-day variations, respectively.

2.2.5 Accuracy, recovery and measurement uncertainty

Trueness is defined as the measurement of the deviation of a measured value to the actual value of an analyte in a sample. Therefore, this parameter demonstrates the bias in an analytical method. The lack of trueness would indicate the presence of systematic error within the method, which renders the method impractical for its intended purpose. Given the absence of certified reference materials for volatile analyses, trueness in the current validation study is expressed as the recovery rate in the spike-and-recovery trial. All spike-and-recovery tests were conducted using a vintage 2020 Marlborough Sauvignon Blanc wine, apart from those of amyl acetate, for which a vintage 2021 Marlborough Sauvignon Blanc wine was used. The total concentration of a volatile compound in its spiked sample was controlled such that it still falls within the calibration range.

2.2.6 Examination of competitive ionization effects

As previously highlighted by Borsdorf and Eiceman, as multiple compounds of different ionization energies (IE) or proton affinities (E_{pa}) enter the IMS ionization chamber simultaneously, competitive ionization could occur such that the compound with lower IE (or higher E_{pa}) becomes preferentially ionized, whereas other compounds are deprived of ions and are thus not eventually detected.[30] This effect was also investigated in the current study where co-elution occurred between 1-propanol and ethyl butyrate. A simulated matrix was prepared with the concentration of 1-propanol maintained at 12 ppm in a 5 mL model solution. Ethyl butyrate was incrementally spiked into the simulated matrix from 0 to 660 ppb to inspect the change of signal intensities in 1-propanol and ethyl butyrate peaks.

2.3 Instrumentation and method parameters

Instrumentation and method details were the same as reported in a previous publication.[11] The G.A.S. FlavourSpec SHS-GC-IMS system was used in the current study (Gesellschaft für Analytische Sensorsysteme mBH, Dortmund, Germany). The instrument was fitted with a MXT-WAX polar column (30 m length × 0.53 mm internal diameter × 0.5 µm film thickness, 100% crossbond Carbowax polyethylene glycol stationary phase) purchased from RESTEK (Bellefonte, PA, USA). An autosampler (CTC Analytics AG, Zwingen, Switzerland) was also connected for the automated static headspace sample introduction on the GC column.

For sample preparation, five milliliters of each prepared sample were transferred into a 20 mL headspace vial using a micropipette, which was then purged with nitrogen and tightly crimped. Each sample vial was incubated at 40 °C for 10 minutes for equilibration, before 500 µL of the headspace gas was extracted with a heated (80 °C) syringe and injected through a heated injection port on the GC column. The GC column was set in isothermal mode at 40 °C. In GC, the carrier gas flow was first held steady at 2 mL/min for one minute, and then gradually increased to 40 mL/min at a rate of 2 mL/min^2 until 20 min. The flow was then immediately increased to 150 mL/min and held at this rate until 50 min. From 50 to 52 min, the flow rate was dropped to 2 mL/min again, before the program finished.

Following GC separation, the compounds were first ionized in the IMS ionization chamber using a tritium (^{3}H) source. The ionization was conducted under positive ion mode. Ionized volatile compounds then entered the IMS drift tube (98 mm), where an electric field (strength: 500 V/cm) was applied. The IMS device was programmed at 75 °C with a constant drift gas flow rate of 150 mL/min counter-current of the analyte ion swarm. Each IMS spectrum was acquired as the average of six scans.

Also, as a critical component of regular instrument upkeep, an intermittent 4-hour thermal cleaning was performed at the conclusion of each sample sequence and a 24-hour thermal cleaning was performed each week over the weekend, which has been shown to reduce memory effects of the GC column and ensure the consistent and desirable analytical results.

2.4 Data processing and statistical analyses

The software suite distributed with the SHS-GC-IMS instrument, LAV (Laboratory Analytical Viewer, version 2.2.1, Dortmund, Germany), was used to process the raw data acquired from each run. The LAV-quantitation module was used to obtain the signal intensities of each volatile compound as peak *volume-under-the-shape*. Microsoft Excel 2019 (Redmond, WA, USA) was used to collate raw data and perform basic calculations such as limits of detection and quantification. The programming language R (version 4.0.2, Vienna, Austria) and Python (version 3.8.3, Fredericksburg, VA, USA) was used to run ANOVA analyses, generate plots, compute the standard curves of Boltzmann function and GAM. For all *post-hoc* Tukey's HSD tests for ANOVA, the significance level was set at 5%.

3 Results and Discussion

3.1 Overall quality control of the method

As shown above in **Table 1**, most quantification studies did not report specifically the involvement of internal standards during method calibration or in quantitative analyses. However, ensuring the quality of semi-quantitative information obtained from SHS-GC-IMS is a crucial first step in checking for intrinsic sources of error that might lower the creditability of the final quantitative results. Hence, a method for monitoring the instrument performance was established using an internal standard spiking solution. Variations in internal standard signals could reveal the perturbations caused by a series of sources of errors, such as operator's pipetting error, autosampler injection, and GC column conditions. The internal standard was selected such that it did not interfere or react with any compounds that inherently exist in the target matrix, while also belonging to one of the same chemical categories as the target compounds of analysis.[31]

Based on these criteria, 3-octanol was selected in the current study as the internal standard and was mixed with samples in 1:100 ratio to achieve a final concentration in the sample of 10-15 ppm. The peak for 3-octanol was well separated from those of the intrinsic volatile compounds (**Supplementary Figure 1**). Also, being a member of the higher alcohols group and thus sharing similar ionization behaviors, excessive fluctuations in the 3-octanol peak signal, if any, could reflect potential inaccuracy in analyzing wine volatile compounds. Two batches of internal standard solution were prepared during the current study, with concentrations of 12.6 ppm and 14.0 ppm, which were used to spike 240 and 139 samples in the timespan of 6 months, respectively. A control chart was plotted for each of the two batches as shown in **Figure 2** (A) and (B). The average signal intensity values of the first and the second internal standard batches were 18889±2070 and 21082±2886, with relative standard deviations (RSD) being 11.0% and 13.7%. Hence, the stability of the method was demonstrated by possessing % RSD lower than 15%. Also, it can be seen from the control chart that in both batches, only eight points (2.1% of all samples) fell within the warning range (shown as red shaded region) and no point fell beyond the control limits, which further consolidates the suitability of the current method in volatile analyses.

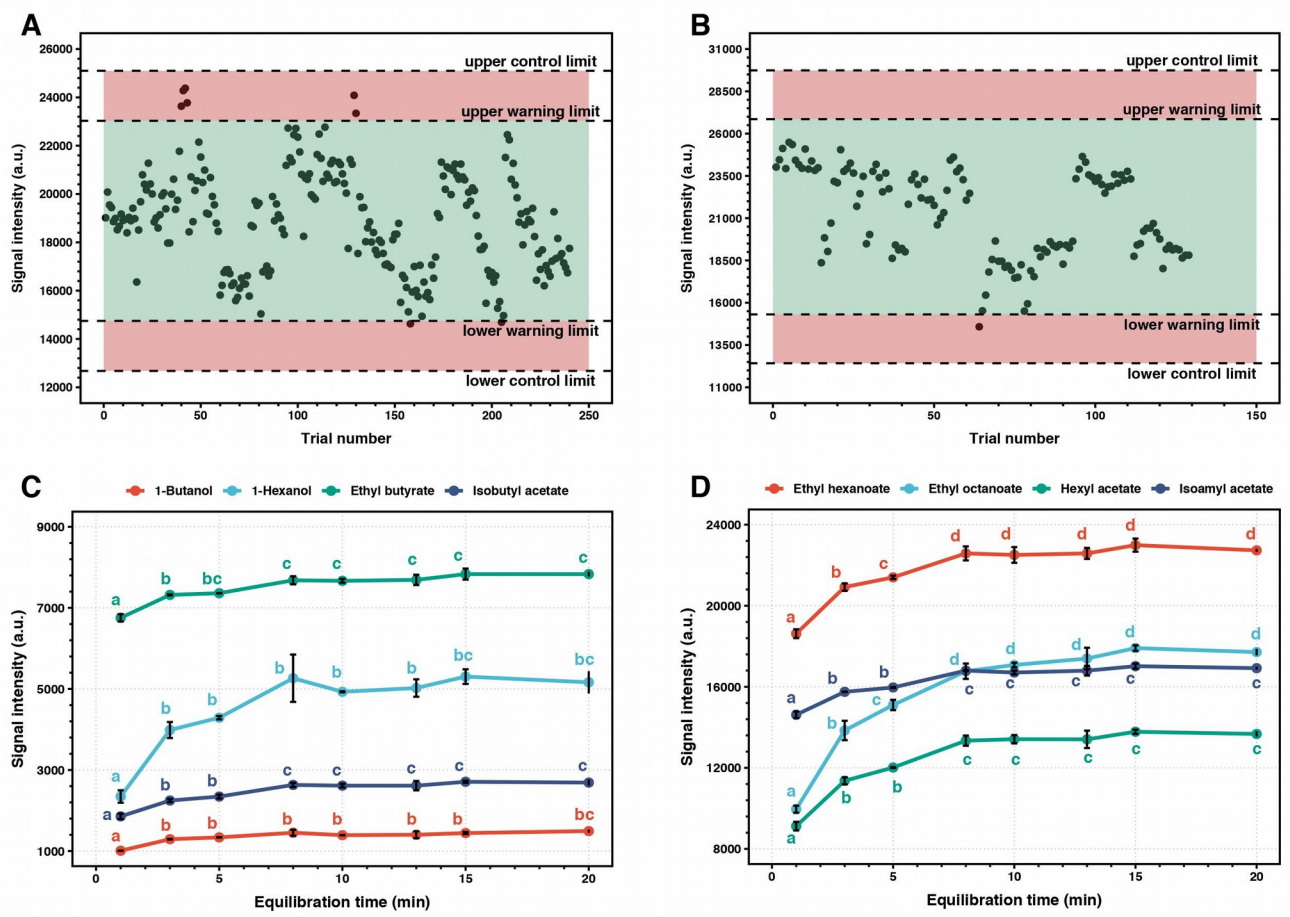

Figure 2.(A) & (B): Control charts of the first and the second batches of internal standard. Upper/lower control limit = mean value ± 3×standard deviation. Upper/lower warning limit = mean value ± 2×standard deviation. (C) & (D): Changes in the signal intensity of peaks of eight representative compounds after incubation for 2- 20 minutes. Points with the different letters on each line indicate statistically significant difference in signal intensities (Tukey's HSD, α=0.05).

By contrast, the HS-SPME-GC-MS method that was developed at the University of Auckland indicated much higher level of RSD in the 3-octanol internal standard signals during method calibration (21.8-37.5%, unpublished results). Such a difference could be explained, at least partially, by the fact the static headspace extraction in the SHS-GC-IMS instrument is a bi-phase system, where only one partition occurs between the liquid fraction of the sample and the gaseous headspace. On the other hand, when pre-concentration devices such as SPME fibers are being used, a tri-phase system is established, where partition can occur between liquid sample and the headspace, as well as between the headspace and the SPME fiber. Therefore, increased instability is introduced into the HS-SPME-GC-MS method as samples are incubated for a fixed amount of time regardless of equilibria between the three phases. Rather, in SHS-GC-IMS, it has been experimentally shown that equilibrium between liquid sample and headspace is reached after 10 minutes of incubation and agitation (see **Figure 2** (C) and (D).). This phenomenon in turn indicates that stable results can be expected after headspace equilibrium is established.

In addition to analytical output monitoring, the internal standard was also used for manually adjusting the chromatograms should deviations on the retention time axis occur. The LAV software that accompanies the GC-IMS instrument allows the user to configure "area sets", *i.e.*, pre-defined boxes to accommodate peaks on the contour plot. It is quite commonly observed that misaligned chromatograms have peaks of both intrinsic compounds, and the internal standard is partially or entirely located outside of their corresponding boxes. In manual alignments, correction to relocate the misaligned IS peak back to its box could also move all other peaks

back to their correction positions, which is critical for the software to correctly extract the peak signal intensities. This approach was also recommended by Jurado-Campos, Martín-Gómez, Saavedra and Arce, who reported that using internal standard as a base for plot alignment could apparently improve the homogeneity of peak positions.[1]

3.2 Selection of standard curve fitting methods

3.2.1 Hurdles in curve-fitting: non-linearity and multiple ion species

One of the most distinct features that immediately differentiate IMS from other commonly used GC detectors is its narrow linear dynamic range and the non-linear response commonly observed when a series of concentrations is used to construct a standard curve. For example, a concentration-response scatter plot of ethyl hexanoate, a common volatile found in wine, for which clear non-linear relationship was identified, is provided in **Figure 3** (A). Around the lower concentrations, the concentration-signal relationship was more linear, whereas the signal became more plateaued as the concentration increased, leading to curvature across the normal concentration range of this compound in the target matrix. This effect has been widely reported for many other compounds as well.[15, 22, 24] One potential solution to circumvent this issue is dilution of the original sample so that the concentration of the target compound is lowered to reach its linear dynamic range.[32]

However, as wine is a highly complicated system consisting of multiple volatile compounds of interest, each with its own linear range and non-linear curvature, it would be exceedingly arduous to analyze even one sample with multiple dilution factors so that all volatiles would fall within their desired linear range. As a result, previous efforts have been made to use various mathematical relationships, including polynomial, logarithmic, and Boltzmann functions, to circumvent this problem using dilutions and to directly account for the non-linear relationship.[15-16, 18] Currently, no consensus has been achieved regarding the mathematical function that best describes this curvature. In this study, the recommended mathematical model by the manufacturer: Boltzmann function, was first trialed (**Figure 3** (B)), followed by the non-parametric fitting method of generalized additive model (GAM) (**Figure 3** (C)), as exemplified using ethyl hexanoate.

As the complexity of fitting model increased, the fitting error decreased accordingly. The linear fitting was consistently problematic at both lower and higher concentrations. The Boltzmann fitting exhibited improvement at the lower concentration end whereas for the higher concentrations, there was still a drift away from the ideal model. The GAM fitting performed the most desirably, as no severe deviation from the ideal model was observed. This downward trend in the lack-of-fit was measured by the decreasing root mean squared error of calibration (RMSE) values (**Figure 3** (D)).

Furthermore, an additional benefit of GAM compared to other fitting methods is its ability to accept multiple input variables when constructing the fitting, which becomes particularly useful when multiple ion species exist for one compound. Hence, for these compounds, the GAM method was tested both on the monomer/dimer pair and on the dimer only. These proposed methods could thus solve the problem of non-linear response behavior and multiple ion species in GC-IMS detection.

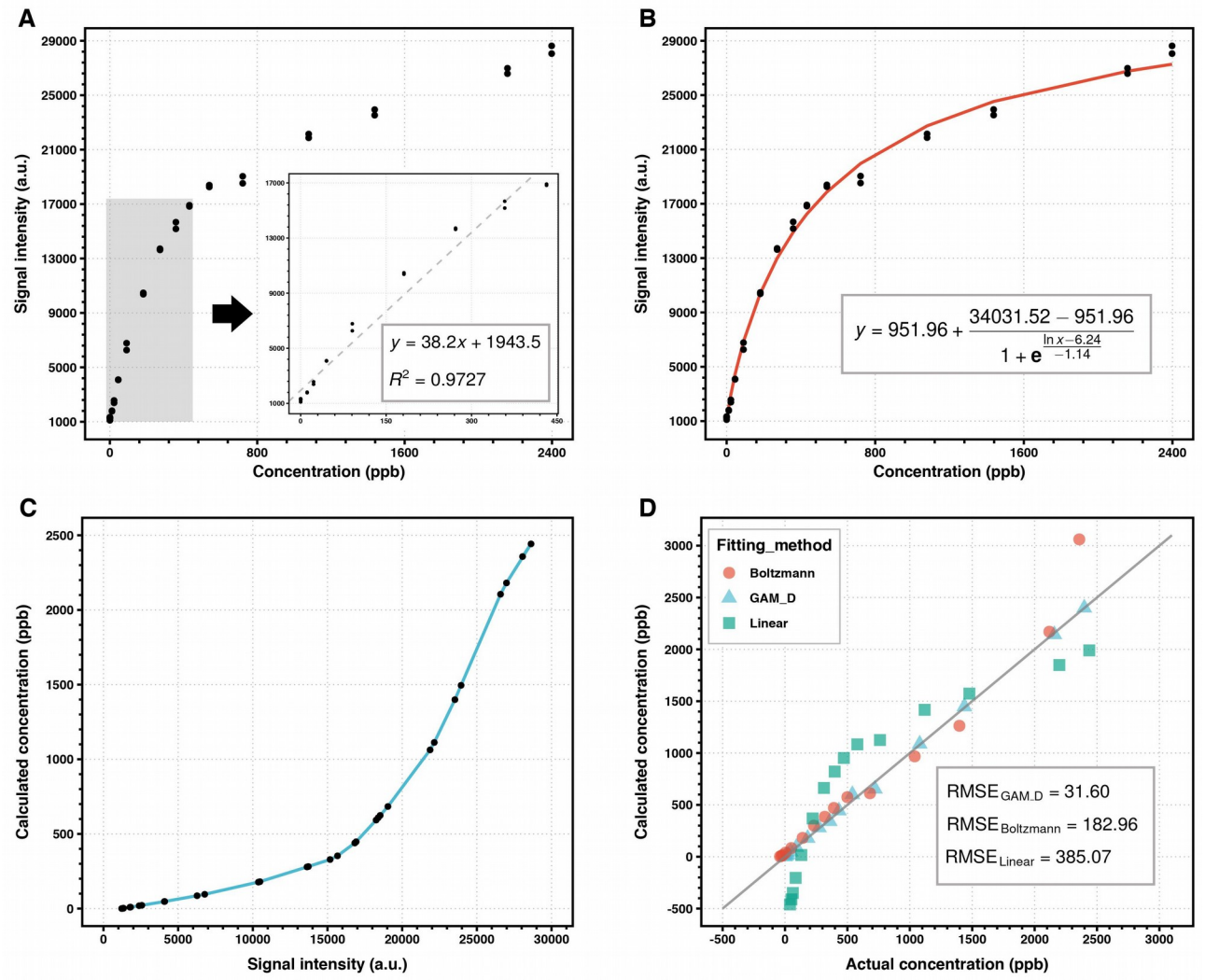

Figure 3.(A): Scatter plot of the calibration data points obtained for ethyl hexanoate using SHS-GC-IMS. The insert shows the region where linearity is still maintained. (B): Fitting of Boltzmann function to the ethyl hexanoate calibration points with the fitted equation. In this equation, y represents the signal intensity (a.u.) and x represents the actual concentration (ppb). (C): Fitting of GAM using b-spline functions to the ethyl hexanoate calibration points. (D): Fitting accuracy of three different methods: Boltzmann function, generalized additive model (GAM), and linear function (GAM_D indicates dimer only used for GAM). The grey line represents the ideal model, from which increased departure intuitively indicates less reliable fitting. The goodness-of-fit is compared across different methods using root mean squared error of calibration (RMSE) as a unified metric.

3.2.2 Comparison of the goodness-of-fit

In order to more comprehensively compare the accuracy of the different fitting methods, a compendium of the RMSE and systematic bias values of the three fitting methods for all studied compounds is presented in **Table 2**. The GAM fitting results were invariably better than Boltzmann and linear fittings, as demonstrated by lower RMSE values, apart from that of ethyl decanoate where GAM performed slightly less favorably. Extremely small systematic bias figures also indicate that no severe under- or over-estimation was expected. Additional involvement of the monomer in the GAM, however, did not necessarily produce significantly improved fitting performance compared to the GAM fitting using only the dimer. This was also shown by the *p*-value of the monomer term coefficients, as only that of 1-hexanol was below 0.1. The Boltzmann function fitting also provides a desirable alternative to GAM, despite its higher general over-estimation in the quantitative results than the GAM model. Nevertheless, such systematic bias is still acceptable considering the wide calibration range used.

However, the GAM method is not without its problems. One of the most prominent difficulties in applying the GAM method lies in the fact that it directly reads the trend from the data per se, thereby rendering the final output greatly prone to any experimental errors from collecting the calibration data. This could result in unusual local maxima/minima in the fitted curve and thus break the monotonicity principle in the concentration-signal relationship, as exemplified by 1-butanol (see **Supplementary Figure 2**). Hence, visual inspection of the fitted curve needs to be exercised when GAM is being used to establish the standard curve. In this case, either the corresponding calibration concentrations may be re-conducted where experimental errors can be clearly identified, or parametric models, *i.e.*, the Boltzmann function may be used instead.

In light of the aforementioned results, it was decided that for this study, both GAM and Boltzmann function fitting would be evaluated in the subsequent figures of merit calculations. In the case of GAM being unable to produce reliable fitting curves, the Boltzmann function should be used instead as a fallback alternative.

Table 2. RMSE and systematic bias figures of GAM, Boltzmann function fitting and linear fitting on the calibration points of the studied volatile compounds in wine. Units for the reported figures are ppb unless otherwise specified.

Compound	Calibration range	GAM_M,D [a]		GAM_D [b]		Boltzmann function		Linear function	
		RMSE	Bias	RMSE	Bias	RMSE	Bias	RMSE	Bias
Methyl acetate	0 – 687.77	—	—	10.81	-5.14×10^{-13}	12.24	0.52	62.35	1.1×10^{-13}
Propyl acetate	0 – 694.39	10.27	-4.37×10^{-10}	10.62	2.20×10^{-13}	11.74	0.25	169.66	154.04
Isobutyl acetate	0 – 712.80	5.05	7.70×10^{-10}	5.32	6.40×10^{-13}	7.45	0.28	101.06	-7.37×10^{-14}
Isoamyl acetate	0 – 6732.0	—	—	59.65	-4.13×10^{-11}	167.78	12.87	1062.09	-3.77×10^{-13}
Amyl acetate	0 – 807.84	—	—	16.88	3.5×10^{-12}	30.28	1.68	93.09	0
Hexyl acetate	0 – 1544.4	—	—	17.47	-2.72×10^{-14}	43.85	4.64	183.95	-1.33×10^{-13}
Ethyl isovalerate	0 – 618.14	—	—	3.20	7.00×10^{-14}	9.63	0.94	79.54	-5.26×10^{-14}
Ethyl 2-methylbutyrate	0 – 620.40	—	—	3.34	-1.63×10^{-12}	11.17	1.40	90.75	0
Ethyl propionate	0 – 495.00	15.33	1.80×10^{-13}	15.04	1.60×10^{-13}	19.47	0.61	64.72	1.50×10^{-14}
Ethyl butyrate	0 – 1029.6	—	—	14.55	6.50×10^{-12}	19.74	0.25	159.63	-1.26×10^{-13}
Ethyl hexanoate	0 – 2398.0	—	—	31.60	3.30×10^{-12}	182.96	23.87	385.07	7.60×10^{-14}
Ethyl octanoate	0 – 3009.6	45.05	1.10×10^{-9}	44.45	2.80×10^{-14}	51.13	1.33	140.11	1.50×10^{-14}
Ethyl decanoate	0 – 1039.5	—	—	19.30	1.40×10^{-8}	18.94	0.39	19.33	-9.58×10^{-15}
Isobutanol [c]	0 – 167.81	0.84	9.59×10^{-13}	0.86	9.22×10^{-13}	3.70	0.60	25.38	-2.10×10^{-15}
1-Butanol [c]	0 – 62.04		*GAM broke monotonicity*			4.96	0.26	12.86	6.00×10^{-15}
Isoamyl alcohol [c]	0 – 329.65	1.17	6.40×10^{-13}	2.55	-4.80×10^{-13}	26.54	4.63	64.56	0
1-Hexanol	0 – 3626.75	16.15	9.00×10^{-10}	30.98	-6.57×10^{-13}	80.70	0.98	79.99	1.20×10^{-13}

a) The GAM method using both monomer and dimer signals;

b) The GAM method using the dimer signal only;

c) Units for the metrics related to these compounds are ppm.

3.3 General figures of merit (FOM) of the method

3.3.1 Limit of detection (LOD) and limit of quantification (LOQ)

Using the methods described in the Materials and Methods section, the limit of detection (LOD) and limit of quantification (LOQ) were calculated for the 17 compounds studied in the simulated wine matrix.

It should be noted that the IUPAC-recommended method was not suitable for the Boltzmann-based standard curves, since sometimes the signal intensities acquired from blank samples are unable to return a valid concentration using this type of model. This is attributed to the fact that the Boltzmann features a sigmoidal curve with upper and lower asymptotes of $y = a$ and $y = b$, respectively (a and b being coefficients of the fitted Boltzmann function). Hence, any signal that falls outside the (b, a) range is not able to return a valid calculated concentration. It is not uncommon that in blank samples, the signal intensity of a given compound is lower than the coefficient b. Therefore, all LOD and LOQ values were calculated using the method proposed by Hayashi *et al*. and González *et al*. for Boltzmann function models.

The LOD and LOQ values of the different non-linear fitting methods are collated in **Table 3**. Due to the different methods used to calculate the LOD and LOQ, these values tend to be higher for Boltzmann function models, which also renders them not directly comparable with those of GAM methods. Nevertheless, it could still be seen that both GAM and Boltzmann function are able to show desirable detection and quantification limits for all compounds studied, considering the calibration ranges applied in this study and their regular presence in wines.[33-35] The use of GAM on the monomer/dimer pair did improve those limits compared to GAM being applied on dimer alone for some compounds, including propyl acetate, ethyl octanoate, and 1-hexanol. This trend, however, did not hold true for all compounds. Also, it could be shown from the both LOD/LOQ value and the RMSE values that the models with better fits (smaller RMSE) are likely to have higher detection/quantification limits, which indicates compromises were made to enhance the general fitting precision in exchange for the model performance at the lower end.

Table 3. LOD and LOQ figures of GAM and Boltzmann function fitting on the calibration points of the studied volatile compounds in wine. Units for the reported figures are ppb unless otherwise specified.

Compound	Calibration range	GAM_M,D [a]		GAM_D [b]		Boltzmann function	
		LOD	LOQ	LOD	LOQ	LOD	LOQ
Methyl acetate	0 – 687.77	—	—	13.32	37.87	13.93	22.77
Propyl acetate	0 – 694.39	3.42	8.26	3.34	10.92	6.39	10.56
Isobutyl acetate	0 – 712.80	3.33	10.01	0.04	0.30	4.70	9.55
Isoamyl acetate	0 – 6732.0	—	—	1.58	2.35	26.14	70.16
Amyl acetate	0 – 807.84	—	—	2.06	3.64	12.02	17.32
Hexyl acetate	0 – 1544.4	—	—	6.93	18.81	40.23	64.56
Ethyl isovalerate	0 – 618.14	—	—	0.27	1.11	5.66	10.10
Ethyl 2-methylbutyrate	0 – 620.40	—	—	0.07	0.35	4.68	8.47
Ethyl propionate	0 – 495.00	4.05	13.28	0.71	0.58	22.44	62.68
Ethyl butyrate	0 – 1029.6	—	—	0.41	1.29	2.49	5.36
Ethyl hexanoate	0 – 2398.0	—	—	5.60	14.85	36.18	65.52
Ethyl octanoate	0 – 3009.6	29.77	82.56	58.67	148.79	188.00	276.36

Ethyl decanoate	0 – 1039.5	—	—	33.96	74.99	82.60	119.11
Isobutanol [c]	0 – 167.81	0.14	0.46	0.10	0.28	1.07	2.53
1-Butanol [c]	0 – 62.04	—	—	—	—	0.26	0.38
Isoamyl alcohol [c]	0 – 329.65	1.46	4.27	0.20	0.59	1.19	2.85
1-Hexanol	0 – 3626.75	40.10	119.95	118.41	300.34	173.69	229.64

a) The GAM method using both monomer and dimer signals;

b) The GAM method using the dimer signal only;

c) Units for the metrics related to these compounds are ppm.

3.3.2 Method precision and accuracy

The precision of quantification models was demonstrated in terms of repeatability (intra-day variation) and reproducibility (inter-day variation). As can be seen from **Figure 4** (A), the precision values of most compounds were below 10% using either of the three quantification models, which indicated desirable robustness of both the analytical and the quantitative calculation methods.

It was also immediately recognizable, however, that the precision of ethyl decanoate was notably worse than that of other compounds. It was revealed by further investigation that for each day, the ethyl decanoate signal in the first analyzed sample was consistently lower than that in subsequent samples. Such a phenomenon could be due to the fact that the instrument was always thermally cleaned at 80 °C at the end of each day, which was essential to minimize retention time and drift time variations as the instrument operates under isothermal GC mode.[11] The cleaning process also clears the column from residual apolar compounds that were unable to detach from the column before the end of each run, which, conversely, was not executed between samples and could thus increases the stationary phase hydrophobicity. A close inspection of the physiochemical properties of ethyl decanoate highlighted that its *log P* value is in the range 3.61-4.43, which infers a stronger tendency to interact with the hydrophobic phase.[36] Therefore, ethyl decanoate signals were less pronounced in the first sample of each day. This finding also showed the need to treat the quantification results of ethyl decanoate with care should the compound be detected in the first analyzed sample after the instrument undergoes thermal cleaning.

The accuracy of quantification was expressed in terms of the recovery of compounds in spiked samples, as collated in **Figure 4** (B). Most compounds were able to receive a recovery value in the range of 60-120% with an average of 74.7%, which indicated an acceptable level of method accuracy. Ethyl propionate and isoamyl alcohol, on the other hand, returned unsatisfactory recovery rates below 60%. Hence, these two compounds were shown unsuitable to be quantified based on the current method.

Additionally, it must also be pointed out that real wine samples contain non-volatile components that have been reported to retain volatile compounds and lower their presence into the headspace, such as polyphenols and polysaccharides.[37-38] Since a simulated matrix was used in the current study, the volatiles in the calibration samples were more likely to be released from the liquid fraction compared to those in real wine samples, which could explain the relatively low recoveries.

For the majority of studied compounds, the three fitting methods achieved similar results. However, a considerable discrepancy in the recovery rates was observed for isobutyl acetate and isoamyl acetate, ethyl isovalerate, and ethyl 2-methylbutyrate. Hence, quantification results from all of Boltzmann, GAM_D and GAM_M,D (if available) should be reported simultaneously, as no single method manifested distinctive superiority over others. Also, future endeavors need to be devoted to identifying the long-term applicability of

these fitting methods by testing them on further matrices and conducting additional calibrations for the compounds of interest.

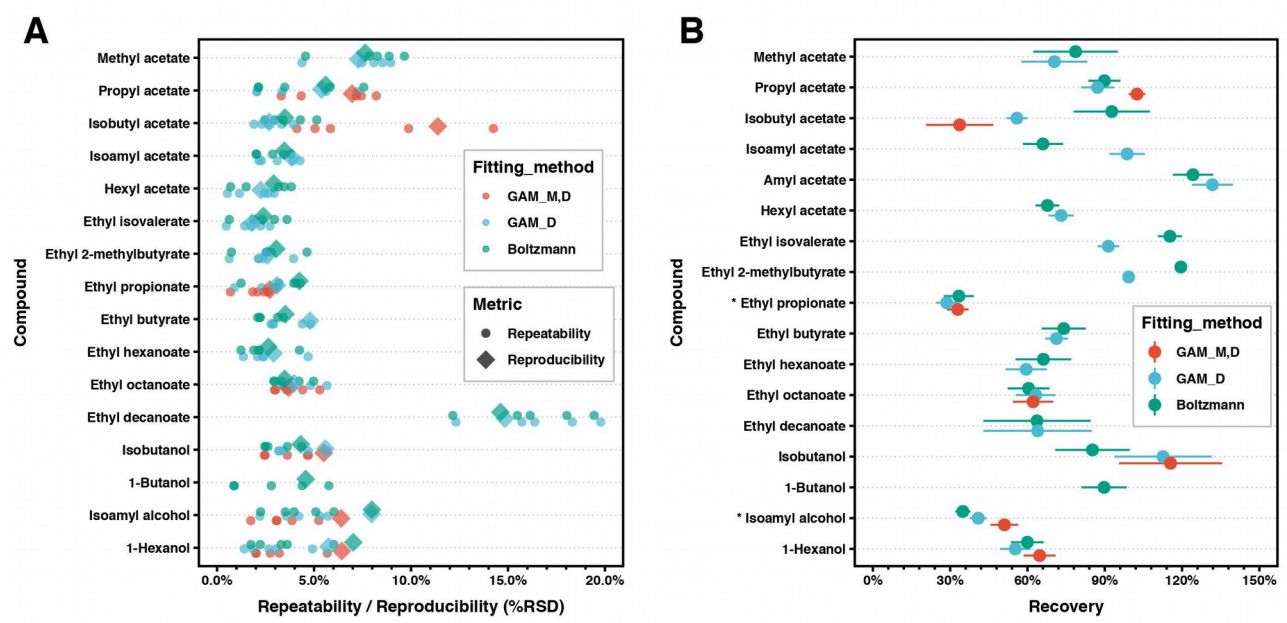

Figure 4. (A): Precision study results of the SHS-GC-IMS method using three different quantification models. (B): Accuracy study results of the SHS-GC-IMS method using three different quantification models. GAM_M,D represents the use of both monomer and dimer ions. GAM_D represents the use of dimer ions only.

3.4 Competitive ionization effects in co-eluting compounds

One of the characteristics that profoundly interferes with the analytical results of IMS-based methods is the competitive ionization between compounds of different ionization energies and proton affinities.[30] This issue has resulted in the tandem use of GC pre-fractionation before the IMS detector to improve the analytical output.[39]

One issue with competitive ionization was observed in the current study between 1-propanol and ethyl butyrate. This effect is seen in the co-evolution curves between a fixed concentration of 1-propanol and varying concentrations of ethyl butyrate (see **Figure 5** (A)). As the addition concentration of ethyl butyrate increased from 0 to 679.8 ppb, the signal intensities of both ion species of 1-propanol dropped significantly by 38.9% and 60.6%, respectively, although this concentration of 1-propanol was maintained at 16.3 ppm throughout the experiment. A closer inspection of the raw chromatogram revealed that the peaks for the two compounds overlap at a retention time of ~300 s, which indicates their simultaneous presence in the IMS ionization chamber (see **Figure 5** (B)). Visual examination of signal peak chromatograms has also showed clear decline in 1-propanol monomer and dimer signal intensities as the ethyl butyrate peak increased (see **Figure 5** (C)).

Such behavior could be explained by different proton affinities (E_{pa}) of the two compounds. The E_{pa} of 1-propanol was reported as 786.5 kJ mol^{-1}.[40] Although no experimental data is available for the E_{pa} of ethyl butyrate, it could be reasonably inferred as being > 833.7–835.7 kJ mol^{-1}, *i.e.*, higher than the E_{pa} of ethyl acetate.[40-41] Hence, the higher proton affinity of ethyl butyrate would result in its preferential ionization while suppressing that of 1-propanol, when the two compounds are simultaneously subject to chemical ionization. However, as the quantitative calibration process was conducted individually for each compound, the calibration model would fail to correctly account for such interaction between ion and lead to the general underestimation of 1-propanol. As a result, 1-propanol quantification was not achieved using the current experimental setup. The competitive ionization phenomenon needs to be considered carefully in the scenario of GC co-elution for future calibration work using GC-IMS, to ascertain the validity of calibration models.

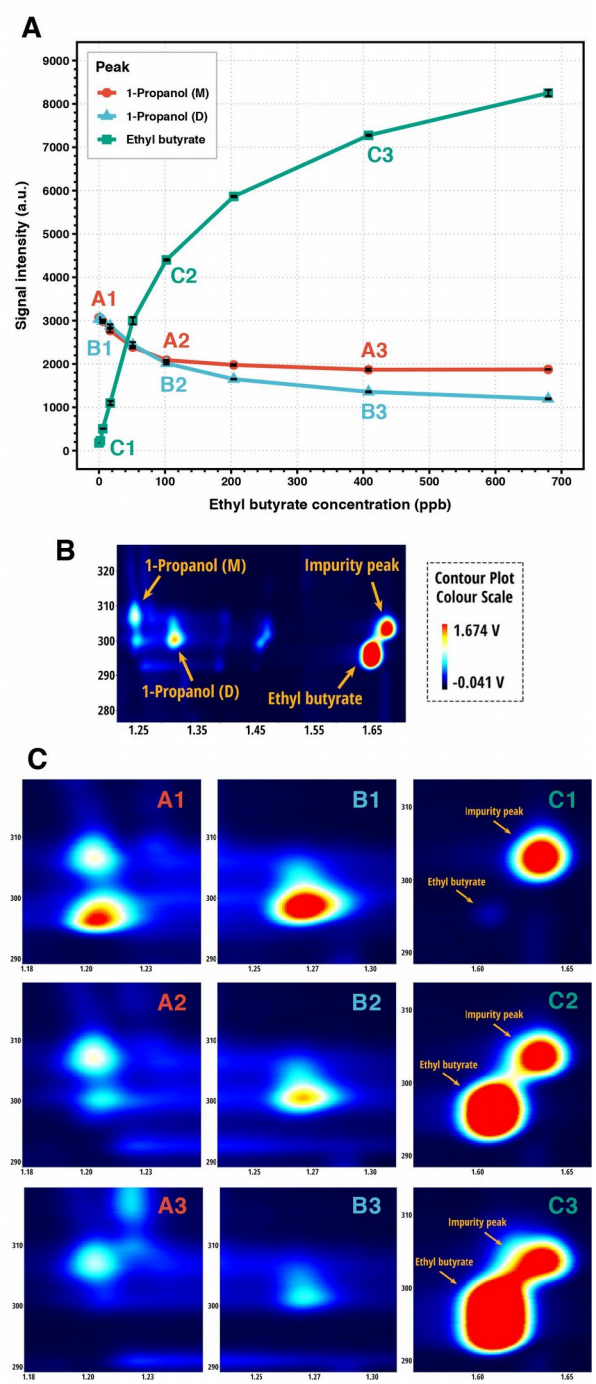

Figure 5. (A): The co-evolution curve between 1-propanol with fixed concentration of 16.3 ppm and ethyl butyrate at 0 to 679.8 ppb. (B): The relative positions of 1-propanol peaks (both monomer M and dimer D) and ethyl butyrate peak. (C): Selected chromatogram snippets of 1-propanol monomer (A1, A2, A3), 1-propanol dimer (B1, B2, B3) and ethyl butyrate (C1, C2, C3). At level 1 (A1, B1, C1), ethyl butyrate concentration = 0 ppb. At level 2 (A2, B2, C2), ethyl butyrate concentration = 51.0 ppb. At level 3 (A3, B3, C3), ethyl butyrate concentration = 407.9 ppb. For all chromatograms in (B) and (C), the X axis represents the drift time (RIP relative) and the Y axis represents the retention time (s).

3.5 Implications between current progress and future improvements

The current study presented an initial approach to establish the great potential of using GC-IMS-based systems for the quantitative analysis of volatile compounds, using wine as an exemplary matrix. Advantages of this method include superior stability and the ease of sample preparation and instrument maintenance. A few

hurdles such as the inevitable non-linearity and occurrence of multiple ion species were tackled using non-linear the Boltzmann fitting function and non-parametric generalized additive model (GAM). Metrics including the goodness-of-fit, limit of detection, limit of quantification, repeatability, reproducibility, and recovery were carefully evaluated. All of the fitting methods were able to return desirable outcomes, while no single method demonstrated apparent superiority over others. Additionally, problems such as competitive ionization need to be promptly identified and mitigated during method optimization to ensure accurate analytical results.

The quantitative capability of GC-IMS shows that it can be employed in addition to its most common use as a simple screening method. This approach offers an alternative to expensive counterparts such as GC-MS, should the absolute concentration of compounds be needed. In commercial winery laboratories, for instance, the instrument with the developed quantitative method could be integrated into the existing routine quality control workflow to provide valuable extra information. Future improvement of GC-IMS quantification could involve validation of the optimal fitting method and the optimization of the elution program to avoid co-elution of compounds to further expand the efficacy of GC-IMS-based quantification.

Acknowledgements

The authors would like to express sincere gratitude towards Constellation Brands, NZ, who kindly supplied us with all the wine samples used in the current study. They would also like to thankfully acknowledge Callaghan Innovation for the financial support (contract number: CONB1801).

Conflict of Interest

The authors declare no competing financial interest.

Supporting Information

This material is available free of charge via the Internet at http://pubs.acs.org.

- Figure S1 Position of the 3-octanol peak on the SHS-GC-IMS chromatogram of a wine sample.
- Figure S2. The GAM fitting curve of 1-Butanol when both monomer and dimer ions were considered.

References

1. Jurado-Campos, N.; Martín-Gómez, A.; Saavedra, D.; Arce, L., Usage considerations for headspace-gas chromatography-ion mobility spectrometry as a suitable technique for qualitative analysis in a routine lab. *J. Chromatogr. A* **2021,** *1640*, 461937.

2. Arroyo-Manzanares, N.; Martín-Gómez, A.; Jurado-Campos, N.; Garrido-Delgado, R.; Arce, C.; Arce, L., Target vs spectral fingerprint data analysis of Iberian ham samples for avoiding labelling fraud using headspace - gas chromatography-ion mobility spectrometry. *Food Chem.* **2018,** *246*, 65-73.

3. Chen, T.; Chen, X.; Lu, D.; Chen, B., Detection of Adulteration in Canola Oil by Using GC-IMS and Chemometric Analysis. *Int. J. Anal. Chem.* **2018,** *2018*, 3160265.

4. Gerhardt, N.; Birkenmeier, M.; Schwolow, S.; Rohn, S.; Weller, P., Volatile-Compound Fingerprinting by Headspace-Gas-Chromatography Ion-Mobility Spectrometry (HS-GC-IMS) as a Benchtop Alternative to (1)H NMR Profiling for Assessment of the Authenticity of Honey. *Anal. Chem.* **2018,** *90* (3), 1777-1785.

5. Ge, S.; Chen, Y.; Ding, S.; Zhou, H.; Jiang, L.; Yi, Y.; Deng, F.; Wang, R., Changes in volatile flavor compounds of peppers during hot air drying process based on headspace-gas chromatography-ion mobility spectrometry (HS-GC-IMS). *J. Sci. Food Agric.* **2020,** *100* (7), 3087-3098.

6. Li, H.; Jiang, D.; Liu, W.; Yang, Y.; Zhang, Y.; Jin, C.; Sun, S., Comparison of fermentation behaviors and properties of raspberry wines by spontaneous and controlled alcoholic fermentations. *Food Res. Int.* **2020,** *128*, 108801.

7. Li, X.; Wang, K.; Yang, R.; Dong, Y.; Lin, S., Mechanism of aroma compounds changes from sea cucumber peptide powders (SCPPs) under different storage conditions. *Food Res. Int.* **2020,** *128*, 108757.

8. Gerhardt, N.; Birkenmeier, M.; Sanders, D.; Rohn, S.; Weller, P., Resolution-optimized headspace gas chromatography-ion mobility spectrometry (HS-GC-IMS) for non-targeted olive oil profiling. *Anal. Bioanal. Chem.* **2017,** *409* (16), 3933-3942.

9. Martín-Gómez, A.; Arroyo-Manzanares, N.; Rodríguez-Estévez, V.; Arce, L., Use of a non-destructive sampling method for characterization of Iberian cured ham breed and feeding regime using GC-IMS. *Meat Sci.* **2019,** *152*, 146-154.

10. Gerhardt, N.; Schwolow, S.; Rohn, S.; Pérez-Cacho, P. R.; Galán-Soldevilla, H.; Arce, L.; Weller, P., Quality assessment of olive oils based on temperature-ramped HS-GC-IMS and sensory evaluation: Comparison of different processing approaches by LDA, kNN, and SVM. *Food Chem.* **2019,** *278*, 720-728.

11. Zhu, W.; Benkwitz, F.; Kilmartin, P. A., Volatile-Based Prediction of Sauvignon Blanc Quality Gradings with Static Headspace-Gas Chromatography-Ion Mobility Spectrometry (SHS-GC-IMS) and Interpretable Machine Learning Techniques. *J. Agric. Food Chem.* **2021,** *69* (10), 3255-3265.

12. Liu, J.; Liu, M.; Liu, Y.; Jia, M.; Wang, S.; Kang, X.; Sun, H.; Strappe, P.; Zhou, Z., Moisture content is a key factor responsible for inducing rice yellowing. *J. Cereal Sci.* **2020,** *94*.

13. Gu, S.; Chen, W.; Wang, Z.; Wang, J., Rapid determination of potential aflatoxigenic fungi contamination on peanut kernels during storage by data fusion of HS-GC-IMS and fluorescence spectroscopy. *Postharvest Biol. Technol.* **2021,** *171*, 111361.

14. Wang, S.; Chen, H.; Sun, B., Recent progress in food flavor analysis using gas chromatography–ion mobility spectrometry (GC–IMS). *Food Chem.* **2020,** *315*.

15. del Mar Contreras, M.; Aparicio, L.; Arce, L., Usefulness of GC-IMS for rapid quantitative analysis without sample treatment: Focus on ethanol, one of the potential classification markers of olive oils. *LWT* **2020,** *120*, 108897.

16. Pu, D.; Duan, W.; Huang, Y.; Zhang, Y.; Sun, B.; Ren, F.; Zhang, H.; Chen, H.; He, J.; Tang, Y., Characterization of the key odorants contributing to retronasal olfaction during bread consumption. *Food Chem.* **2020,** *318*, 126520.

17. Thomas, C. F.; Zeh, E.; Dörfel, S.; Zhang, Y.; Hinrichs, J., Studying dynamic aroma release by headspace-solid phase microextraction-gas chromatography-ion mobility spectrometry (HS-SPME-GC-IMS): method optimization, validation, and application. *Anal. Bioanal. Chem.* **2021,** *413* (9), 2577-2586.

18. Budzyńska, E.; Sielemann, S.; Puton, J.; Surminski, A. L. R. M., Analysis of e-liquids for electronic cigarettes using GC-IMS/MS with headspace sampling. *Talanta* **2020,** *209*, 120594.

19. Kwantwi-Barima, P.; Hogan, C. J., Jr.; Clowers, B. H., Deducing Proton-Bound Heterodimer Association Energies from Shifts in Ion Mobility Arrival Time Distributions. *J. Phys. Chem. A* **2019,** *123* (13), 2957-2965.

20. Raza, A.; Song, H.; Begum, N.; Raza, J.; Iftikhar, M.; Li, P.; Li, K., Direct Classification of Volatile Organic Compounds in Heat-Treated Glutathione-Enriched Yeast Extract by Headspace-Gas Chromatography-Ion Mobility Spectrometry (HS-GC-IMS). *Food Anal. Methods* **2020,** *13* (12), 2279-2289.

21. Jin, Y.; Shu, N.; Xie, S.; Cao, W.; Xiao, J.; Zhang, B.; Lu, W., Comparison of 'Beibinghong' dry red wines from six producing areas based on volatile compounds analysis, mineral content analysis, and sensory evaluation analysis. *Eur. Food Res. Technol.* **2021,** *247* (6), 1461-1475.

22. Brendel, R.; Schwolow, S.; Rohn, S.; Weller, P., Comparison of PLSR, MCR-ALS and Kernel-PLSR for the quantification of allergenic fragrance compounds in complex cosmetic products based on nonlinear 2D GC-IMS data. *Chemom. Intell. Lab. Syst.* **2020,** *205*, 104128.

23. Speckbacher, V.; Zeilinger, S.; Zimmermann, S.; Mayhew, C. A.; Wiesenhofer, H.; Ruzsanyi, V., Monitoring the volatile language of fungi using gas chromatography-ion mobility spectrometry. *Anal. Bioanal. Chem.* **2021,** *413* (11), 3055-3067.

24. Denawaka, C. J.; Fowlis, I. A.; Dean, J. R., Evaluation and application of static headspace-multicapillary column-gas chromatography-ion mobility spectrometry for complex sample analysis. *J. Chromatogr. A* **2014,** *1338*, 136-148.

25. Hastie, T.; Tibshirani, R.; Friedman, J., Basis Expansions and Regularization. In *The Elements of Statistical Learning*, 2009; pp 139-189.

26. González-Barreiro, C.; Rial-Otero, R.; Cancho-Grande, B.; Simal-Gándara, J., Wine aroma compounds in grapes: a critical review. *Crit. Rev. Food Sci. Nutr.* **2015,** *55* (2), 202-218.

27. Hayashi, Y.; Matsuda, R.; Ito, K.; Nishimura, W.; Imai, K.; Maeda, M., Detection Limit Estimated from Slope of Calibration Curve: An Application to Competitive ELISA. *Anal. Sci.* **2005,** *21* (2), 167-169.

28. Mocak, J.; Bond, A. M.; Mitchell, S.; Scollary, G., A statistical overview of standard (IUPAC and ACS) and new procedures for determining the limits of detection and quantification: Application to voltammetric and stripping techniques. *Pure Appl. Chem.* **1997,** *69* (2), 297-328.

29. Karpas, Z.; Guamán, A. V.; Calvo, D.; Pardo, A.; Marco, S., The potential of ion mobility spectrometry (IMS) for detection of 2,4,6-trichloroanisole (2,4,6-TCA) in wine. *Talanta* **2012,** *93*, 200-205.

30. Borsdorf, H.; Eiceman, G. A., Ion Mobility Spectrometry: Principles and Applications. *Appl. Spectrosc. Rev.* **2006,** *41* (4), 323-375.

31. Wang, M.; Wang, C.; Han, X., Selection of internal standards for accurate quantification of complex lipid species in biological extracts by electrospray ionization mass spectrometry-What, how and why? *Mass Spectrom. Rev.* **2017,** *36* (6), 693-714.

32. Márquez-Sillero, I.; Aguilera-Herrador, E.; Cárdenas, S.; Valcárcel, M., Determination of 2,4,6-tricholoroanisole in water and wine samples by ionic liquid-based single-drop microextraction and ion mobility spectrometry. *Anal. Chim. Acta* **2011,** *702* (2), 199-204.

33. Antalick, G.; Perello, M.; De Revel, G., Esters in Wines: New Insight through the Establishment of a Database of French Wines. *Am. J. Enol. Vitic.* **2014,** *65* (3), 293-304.

34. de-la-Fuente-Blanco, A.; Sáenz-Navajas, M. P.; Ferreira, V., On the effects of higher alcohols on red wine aroma. *Food Chem.* **2016,** *210*, 107-114.

35. Lyu, X.; Araújo, L. D.; Quek, S.-Y.; Kilmartin, P. A., Effects of Antioxidant and Elemental Sulfur Additions at Crushing on Aroma Profiles of Pinot Gris, Chardonnay and Sauvignon Blanc Wines. *Food Chem.* **2021,** *346*, 128914.

36. Souza, E. S.; Zaramello, L.; Kuhnen, C. A.; S., J. B. d.; Yunes, R. A.; Heinzen, V. E. F., Estimating the octanol/water partition coefficient for aliphatic organic compounds using semi-empirical electrotopological index. *Int. J. Mol. Sci.* **2011,** *12* (10), 7250-7264.

37. Lyu, J.; Chen, S.; Nie, Y.; Xu, Y.; Tang, K., Aroma release during wine consumption: Factors and analytical approaches. *Food Chem.* **2021,** *346*, 128957.

38. Rodríguez-Bencomo, J. J.; Muñoz-González, C.; Andújar-Ortiz, I.; Martín-Álvarez, P. J.; Moreno-Arribas, M. V.; Pozo-Bayón, M. Á., Assessment of the effect of the non-volatile wine matrix on the volatility of typical wine aroma compounds by headspace solid phase microextraction/gas chromatography analysis. *J. Sci. Food Agric.* **2011,** *91* (13), 2484-2494.

39. Vautz, W.; Franzke, J.; Zampolli, S.; Elmi, I.; Liedtke, S., On the potential of ion mobility spectrometry coupled to GC pre-separation - A tutorial. *Anal. Chim. Acta* **2018,** *1024*, 52-64.

40. Hunter, E. P. L.; Lias, S. G., Evaluated Gas Phase Basicities and Proton Affinities of Molecules: An Update. *J. Phys. Chem. Ref. Data* **1998,** *27* (3), 413-656.

41. Holmes, J. L.; van Huizen, N. A.; Burgers, P. C., Proton affinities and ion enthalpies. *Eur. J. Mass Spectrom.* **2017,** *23* (6), 341-350.